

# Chapter 2

## Thin Film Capacitive Sensors

Herman Smit, Rigel Kivi, Holger Vömel and Ari Paukkunen

### 2.1 Introduction: Principle of Operation

Achievements in microtechnology have encouraged the development of a large variety of very small humidity sensors for miscellaneous applications to measure the water vapour content in gaseous systems. Today, more than 75 % of these miniaturised humidity sensors in the market use a capacitive technique (Rittersma 2002). Most of these capacitive sensors are based on dielectric changes of thin films upon water vapour uptake as a measure of the water vapour content. The porous polymer material acts as a hydroactive sponge whereby the water molecules within the polymer material are in thermodynamic equilibrium with the gas phase, i.e. the rate of adsorption of molecules onto the surface is exactly counterbalanced by the rate of desorption of molecules into the gas phase (Anderson 1995). The water adhesion is characterized by physical hydrogen bonds through the “weak” Van der Waals interaction of water molecules with the hydrophilic groups of the polymer molecules (Matsuguchi et al. 1998, e.g.).

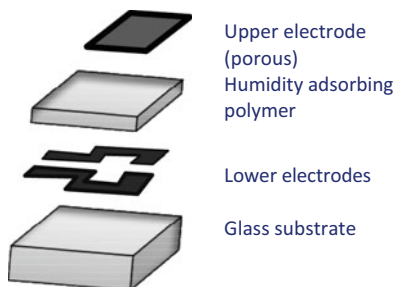
The capacitive thin-film moisture sensor responds to changes of relative, rather than absolute humidity in the surrounding air as well as to changes of temperature. It is, therefore, commonly calibrated in terms of relative humidity (RH). The response time of the humidity sensor is dependent on the polymer’s ability to adsorb and desorb water vapour and on the sensor design, whereby it is strongly dependent on the temperature of the sensor. The sensor is sensitive to chemical contamination by either additional bonding of the non-water molecules or reducing the ability of the polymer to adsorb water molecules, which may cause either a dry bias or reduce the sensitivity of the sensor.

The best known meteorological application is the Humicap sensing element developed by Vaisala (Finland) in 1970’s (Salasmaa and Kostamo 1975), which is being used on their radiosondes since 1980. Based on thin-film technology the sensor consists of a hydroactive polymer film as dielectric between two electrodes applied on a

---

H. Smit (✉) · R. Kivi · H. Vömel · A. Paukkunen  
Research Center Jülich (IEK-8), 52425 Jülich, Germany  
e-mail: h.smit@fz-juelich.de

**Fig. 2.1** The basic principle of the Humicap technology



glass substrate (see Fig. 2.1). Two types of polymer materials have been developed, the A-type and the H-type polymer. The newer H-polymer (introduced in 1990) is more stable and less hydrophilic compared to the A-type polymer. An additional airborne application of capacitive sensors is their deployment on board of commercial aircraft to measure the water vapour concentration between the surface and up to 13 km altitude in the context of the MOZAIC (Measurement of Ozone and Water Vapour by AIRBUS In Service Aircraft). The performance of the humidity sensors made by Vaisala and used on their radiosondes as well as by MOZAIC onboard commercial aircraft are described in this chapter.

## 2.2 Radiosondes

### 2.2.1 Introduction

For nearly 80 years, balloon-borne radiosondes have been the primary source for vertical profiles of atmospheric parameters used in operational weather forecasting and, more recently for climate studies. During balloon ascent, pressure, temperature, humidity and wind are measured from the surface to the lower stratosphere and transmitted to a ground receiving station for further data processing and archiving. A comprehensive overview of radiosondes instruments is given in (WMO 2008). Radiosondes are provided by various manufacturers and deploy different types of relative humidity sensors, such as goldbeater's skin sensors, lithium chloride sensors, carbon hygristors, and thin-film capacitors.

In the early decades of upper air soundings goldbeater's skin (the outer membrane of cattle intestine, which varies in length with changes in relative humidity) and films of lithium chloride on strips of plastic (whose electrical resistance varies with relative humidity) were most commonly used. These sensor types perform poorly at temperatures below  $-20^{\circ}\text{C}$  and suffer from significant hysteresis effects and biases (WMO 2008). Later, plastic or glass strip coated with a hygroscopic film containing carbon particles that changes electrical resistance with relative humidity, called carbon hygristors, were used. However, carbon hygristors suffer from a moist bias at relative humidities above 60% (Schmidlin and Ivanov 1998) and reveal a

pronounced hysteresis after exiting clouds. In general, its performance is unreliable at temperatures below  $-40^{\circ}\text{C}$  or at low relative humidities (WMO 2008). Thin film capacitors, consisting of a hydroactive polymer film between two electrodes are faster and more reliable than carbon hygristors and are the most common type of humidity sensors on radiosondes today. Much of the archived upper tropospheric humidity data for the past several decades are not reliable for climate studies, possibly with the exception of upper tropospheric humidity data from thin-film capacitors (Kley et al. 2000).

The most widely used radiosondes in the global upper-air sounding network have been developed by Vaisala. Since 1980 Vaisala has produced radiosondes using Humicap sensors. These sensors were first integrated into RS80 radiosondes and later into RS90 and RS92 radiosondes. This section provides an overview for each of the Vaisala humidity sensors since the early 1980s including a description of the main changes affecting the long-term humidity data continuity.

### 2.2.2 RS80 Radiosonde

RS80 radiosondes were introduced in 1980. These sondes were first equipped with an A-Humicap sensor. Later these sondes were also available with H-Humicap sensors. The factory calibration procedure relates the measured capacitance to relative humidity with respect to liquid water at  $+20^{\circ}\text{C}$ . RH is calculated from the measured capacitance in two processing steps. First, RH is calculated from the individual calibration curve derived from the calibration of each sensor at  $+20^{\circ}\text{C}$  and at 0% and 75% RH. Second, RH is then adjusted for the measured ambient temperature on the basis of a sensor-type specific temperature-dependence (TD) calibration model, which consists of RH and temperature dependent curve fits derived from a large set of sensors tested at the calibration facility of the manufacturer (Miloshevich et al. 2001).

Most meteorological sensors are calibrated in terms of relative humidity over liquid water (WMO 2008), which is defined as:

$$RH \equiv RH_w = 100 \cdot \frac{e}{e_w(p, T)} \quad (2.1)$$

No data exist for the saturation vapour pressure over liquid water  $e_w(T)$  at low temperatures and theoretical equations describing the saturation vapour pressure over liquid water differ significantly at temperatures less than  $-40^{\circ}\text{C}$ . Therefore it is essential to know the vapour pressure equation used by the manufacturer in their calibration process when using RH measurements at low temperatures. Vaisala uses the formulation by (Wexler 1976) for  $e_w(T)$ . However, other saturation water vapour pressure equations for temperature below  $0^{\circ}\text{C}$  exist (see Appendix B) and were reviewed by for example by (Murphy and Koop 2005).

Production calibration of the RS80 radiosonde A-Humicap sensor relies on the A-type specific calibration model and on linear temperature dependence. Calibration and related corrections have been unchanged between October 1985 and the end

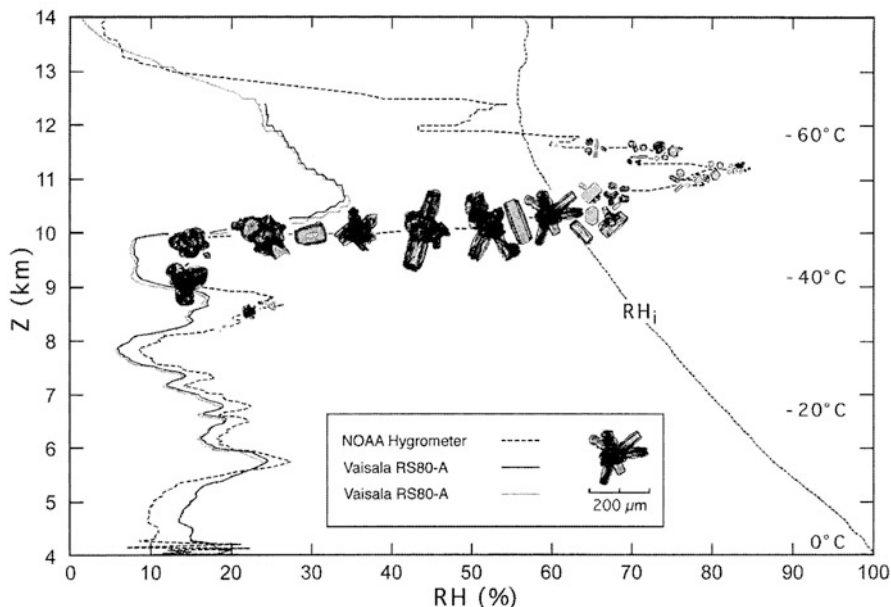


**Fig. 2.2** Altitude profiles of RH (with respect to liquid water) measured simultaneously by the NOAA frostpoint hygrometer and two Vaisala RS80-A radiosondes in a cirrus cloud on 10 Nov 1994 near Boulder, Colorado. Superimposed are simultaneously observed ice crystals. The ice-saturation curve ( $RH_i$ ) and several reference temperatures are also shown. (From Miloshevich et al. 2001, used with permission)

of production in 2008. Production calibration of the RS80 radiosonde H-Humicap sensor uses an H-type specific calibration model, including a nonlinear temperature dependence, which have been unchanged between 1990 and the end of the RS80 production.

Measurements have shown that the temperature dependence of the A-Humicap is, in fact, nonlinear. As a result, the linear correction is insufficient at temperatures below  $-20^\circ\text{C}$  (Miloshevich et al. 2001; Wang et al. 2002), leading to a significant dry bias in RH measurements especially at high humidities. An example of this dry bias inside a cirrus cloud is shown in Fig. 2.2. From a statistical analysis of simultaneous RH measurements from RS80-A radiosondes and the NOAA cryogenic frost point hygrometer (Miloshevich et al. 2001) derived a multiplicative dry bias correction factor of about 1.3 at  $-35^\circ\text{C}$ , 1.6 at  $-50^\circ\text{C}$ , 2.0 at  $-70^\circ\text{C}$ . Thus, the inadequate temperature-dependence (TD) correction is the dominant systematic error in A-type Humicap measurements.

The nonlinear TD correction for H-type RS80 sensors removed large parts of the humidity dry bias found in the A-type Humicap; however a significant dry bias at low temperatures remained: 4 % of the measured RH at  $-40^\circ\text{C}$ , 13 % at  $-60^\circ\text{C}$ , and 32 % at  $-80^\circ\text{C}$  (Wang et al. 2002). Despite the improved calibration, some issues in

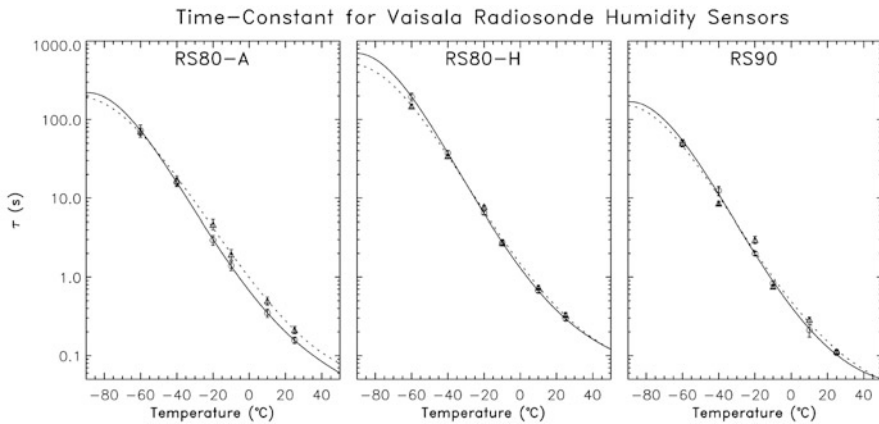


**Fig. 2.3** Response time as function of temperature for the Vaisala RS80-A, RS80-H and RS90 humidity sensors. (From Miloshevich et al. 2004, used with permission)

RS80-H production remained, causing biases and additional batch variations (Turner et al. 2003; Revercomb 2003; Verver et al. 2006).

An additional source of measurement error is caused by sensor lag, i.e. strong smoothing of the RH-profile at lower temperatures. The response time of the RS80 Humicap is mainly dependent on the characteristics of the polymer, sensor and sensor boom design. Laboratory measurements by Vaisala (Miloshevich et al. 2004), adopted from (Paukkunen 2002) show that the response time (63 %) of the Humicap sensor increases approximately exponentially with decreasing temperature, exceeding 1 min. at temperatures colder than about  $-50^{\circ}\text{C}$  (Fig. 2.3). Depending on the sign of the vertical RH-gradient the time lag error can be positive or negative. Statistically, the time lag is expected to produce on the average a zero overall bias if at a given altitude the distribution of increasing and decreasing relative humidity would be symmetric. In reality, the time lag error may contribute a systematic bias at levels with pronounced increasing or decreasing relative humidity, such as at the tropopause.

A time lag correction has been developed by (Miloshevich et al. 2004). A statistical analysis of the difference between time lag corrected RS80-H and simultaneous NOAA-cryogenic frostpoint hygrometer (CFH) shows that the corrections reduced the mean radiosonde dry bias to 4 % RH at  $-20^{\circ}\text{C}$  and 10 % RH at  $-70^{\circ}\text{C}$  to about  $\pm 2$  % RH at all temperatures (Miloshevich et al. 2004).

In addition to time lag for both Humicap sensors and an inappropriate temperature-dependence for the A-Humicap sensor some issues in RS80-H production remained, causing biases and additional batch variations (Turner et al. 2003; Revercomb 2003; Verver et al. 2006). Chemical contamination was found to be an additional source of systematic bias. A major source of contaminating chemical molecules is the radiosonde packaging material, which outgases after the radiosonde has been vacuum-sealed in its foil bag. Contamination may cause a dry bias depending on

sensor type, storing time and storage conditions. The A-Humicap polymer is more selective to water and thereby less sensitive to chemical contamination. The contamination correction for the A-Humicap sensor is estimated to be approximately 2–5 RH %. For RS80-H the contamination correction is estimated in the range of 5–10 RH %, depending on storing time and storage conditions (Wang et al. 2002). RS80 radiosondes produced after June 2000 are not expected to exhibit this error due to a change in packaging using an absorbing material (gradually phased into production starting in September 1998) and a mechanical shield around the sensor boom, which is removed before radiosonde use (in production starting in June 2000). Several studies reported a significant decrease of the dry bias after the introduction of new packaging materials (Wang et al. 2002; Nakamura et al. 2004).

RS80 humidity sensors are shielded with an aluminized protective cap to prevent the impact of solar radiation and precipitation. Despite the shielding, the sensor exhibits a daytime radiation dry bias, which was noted as a sensor arm heating before launch and for a certain time after launch (Wang et al. 2002) and a dry bias in the integrated precipitable water (Turner et al. 2003; Cady-Pereira et al. 2008; Ciesielski et al. 2009).

Condensation and sublimation on the surface of the sensor or on the surrounding mechanical surfaces may also contribute to a microclimate around the sensor. In saturated conditions or in rain a sensor may become contaminated or coated with ice or liquid water and may no longer measure the true ambient RH correctly. RH values that are obviously too high and a lack of sensitivity in fast changes of ambient RH are an indication for sensor icing.

### **2.2.3 RS90 Radiosonde**

The RS90 radiosonde, which was manufactured from 1997 to 2005 introduced a heated H-polymer twin sensor design (Antikainen and Paukkunen 1994; Paukkunen 1995) to make measurements less vulnerable to sensor icing. Due to the smaller sensor size the time response was significantly faster compared to the RS80 sensors. The humidity sensors of this sonde were alternately heated at regular time intervals using a heating resistor integrated into the glass substrate of the sensor. In heating mode a sensor's temperature was raised above the boiling point of water to remove any condensation. After cooling down to ambient temperature, the sensor then continued operating in measurement mode, at which moment the second sensor started its heating cycle. Alternating heating cycles extended down to  $-40^{\circ}\text{C}$  and were not done at lower temperatures. Due to the smaller sensor size the time response was significantly faster compared to the RS80 sensors (see Fig. 2.3).

With the introduction of the RS90 radiosonde a new calibration facility and a new calibration model (Paukkunen 1998) were introduced as well. The calibration was now fitted to several calibration points, directly traceable to reference standards. Batch dependent variations and basic calibration model based biasing (as in RS80 radiosondes) were reduced. Accuracy and performance of RS90 radiosonde have

been described by Paukkunen et al. (2001), who also introduced a new method for the evaluation of uncertainties of radiosonde measurements.

Initially the temperature dependence correction for the humidity sensor was based on the RS80 H-Humicap model. An updated temperature dependence correction was introduced on 25 June 2001. In contrast to the RS80 radiosondes, a contamination protection shield (boom cover) was not used for RS90 radiosonde packages. As a result, increased variations and a possible dry bias in RS90 humidity measurements may have been caused by storage time and conditions (Miloshevich et al. 2006). Also due to the geometry of the sensor, the RS90 humidity sensor does not have a protective rain cap over it. Although this may be considered advantageous with respect to sensor ventilation, the lack of a cap leads to increased sensitivity of the RS90 sensor to solar radiation.

Few detailed comparisons have been done using the RS90 radiosonde. Comparisons of integrated precipitable water from sondes and microwave radiometers showed that the RS90 exhibited a significant daytime dry bias in the lower troposphere (Van Baelen et al. 2005). This relative dry bias was found to be between 6–8 % (Miloshevich et al. 2006), using a smaller sample 2–9 % (Cady-Pereira et al. 2008), and using a number of different stations 5–7 % (Wang and Zhang 2008). This daytime dry bias has not been vertically resolved for the RS90 radiosonde; however, (Vömel et al. 2007a) noted that in a very limited sample the vertically resolved dry bias might not be as large as that for the RS92. However, (Rowe et al. 2008) investigated the RS90 dry bias over Antarctica at lower pressures compared to the other studies and found a dry bias consistent with that by (Vömel et al. 2007a) for the RS92. The radiation error is larger than that for the RS80 (Smout et al. 2000) because of the absence of a protective cap, which had been part of the RS80 humidity sensor. The absence of this protective cap exposes the sensing elements to direct sunlight allowing the sensor temperature to rise significantly above ambient temperature. Furthermore, a larger batch-to-batch variability in the production of RS90 radiosondes may increase the overall uncertainty of humidity measurements using RS90 sondes (Smout et al. 2000).

#### **2.2.4 RS92 Radiosonde**

The latest Vaisala radiosonde model, the RS92, is in use since 2004 and uses a heated dual H-Humicap sensors design similar to that of the RS90. The heating cycles were optimized to prevent sensor icing by tuning the heating parameters and extending the heating cycles from  $-40^{\circ}\text{C}$  to down to  $-60^{\circ}\text{C}$  (introduced since March 2005). In addition the coating of the sensor arm has been improved (Vaisala 2007), which was tested in the Mauritius radiosonde intercomparison (Nash et al. 2006) and entered production in September 2006 and modified in June 2008. The RS92 incorporates a reconditioning cycle before a sounding using the ground check device (model GC25) to remove chemical contamination. The time response of the RS92 humidity sensor is assumed to be the same as the RS90, and time lag errors may still be seen in fast humidity changes at cold temperatures. At the beginning of the RS92 production, the

temperature dependence correction for the radiosonde humidity sensor was based on the RS90 H-Humicap model. A new temperature-dependent (TD) calibration model was implemented in production since April 2004. Changes in the RS92 design have been documented by Vaisala and can be identified with the help of the radiosonde serial number (Vaisala 2009).

First RS92 radiosondes were tested during radiosonde campaigns in 2003–2004 (Miloshevich et al. 2006; Vömel et al. 2007a, b; Suortti et al. 2008). The sondes participated in the WMO radiosonde intercomparison campaign at Mauritius in 2005 (Nash et al. 2006) and later in a number of field campaigns (Suortti et al. 2008; Vömel et al. 2007a, b; Miloshevich et al. 2006, 2009; Nuret et al. 2008). Similar to previous studies the following sources of RS92 humidity measurement uncertainty should be considered (Miloshevich et al. 2009): mean calibration bias, solar radiation error in daytime measurements, random production variability, sensor time-lag error, ground check related uncertainty, and round off error in the standard RS92 processed data files. Time-lag and empirical bias corrections are expected to improve the humidity measurements of operationally launched RS92 sondes.

In daytime measurements the radiation dry bias is the dominant systematic error. It is strongly altitude dependent due to the decrease in convective cooling of the sensor and may reach up to 50 % of the measured relative humidity in the tropical upper troposphere (Vömel et al. 2007a; Yoneyama et al. 2008).

In nighttime soundings the radiation error does not play a role and only calibration and measurement errors of the sensor itself contribute. (Miloshevich et al. 2009) found that in the lower troposphere the RS92 shows a moist relative bias between 3 % for moist conditions and up to 20 % for dry conditions (both at 700 hPa). The moist bias is also indicated in pre-launch ground tests under saturated conditions, and shows a strong dependence on the production-batch. In the upper troposphere this changes to a dry relative bias between 5 % for moist conditions and up to 20 % for dry conditions (Miloshevich et al. 2009).

The time lag smoothes out sharp vertical features and only leads to systematic biases in climatological records, where the RH profile is always decreasing, i.e. above the tropopause. However, the time lag will reduce the measurement uncertainty for individual profiles and increase the significance in larger data sets.

During the ground check the RH sensors are sealed in a small chamber filled with a desiccant and assumed to be at 0.0 % RH. Laboratory tests of different desiccants indicate that the best desiccant may only achieve an RH of 0.5 % (Gorman 2002), which coincidentally is near the average correction applied with well-maintained ground check units. Great care has to be taken that the desiccant has been properly dried, since the ground check value may represent the largest source of measurement uncertainty at low RH values.

After the correction of all systematic biases and time lag error RS92 data may have a bias uncertainty which is independent of height or RH and is estimated to be  $\pm 4$  % RH for nighttime soundings and  $\pm 5$  % for daytime soundings, plus an RH offset uncertainty of  $\pm 0.5$  % RH that is significant for dry conditions (Miloshevich et al. 2009). The uncertainty in the reference observations is one of the contributions to these uncertainty estimates and already included in these estimates.

### 2.2.5 Summary

Radiosondes deploying thin film capacitive sensors have the ability to provide humidity data that may be used for long term climate studies. The most widely used capacitive sensor is the Humicap (A- or H-type) developed by Vaisala and integrated in their radiosondes. Since 1980 the RS80 sondes have been equipped with the A-type (RS80-A) and the more stable and less hydrophilic H-type polymers, while the RS90 and RS92 sondes have been equipped only with the H-type polymer. The Humicap sensor responds to changes of relative humidity with respect to liquid water with a precision of  $\pm 1\%$  RH for Humicap-A and  $\pm 0.5\%$  RH for Humicap-H. An overview of factors affecting humidity measurements using Vaisala RS80-A, RS80-H, RS90 and RS92 sondes is shown in Table 2.1. The differences and correction methods of the humidity measurements by these widely used radiosondes have been described by (Suortti et al. 2008) and (Miloshevich et al. 2009).

The Humicap sensors are calibrated at the factory applying different temperature dependent (TD) calibration models for the RS80-A, RS80-H, RS90 and RS92 sondes, respectively. Due to an inadequate linear TD-calibration model RS80-A humidity measurements show a strongly increasing dry bias with decreasing temperature. Although, the use of a non-linear TD-calibration model for the Humicap-H type sensors have reduced large part of these dry bias effects at lower temperatures, a significant dry bias remains. The most often used dry bias corrections for the RS80 humidity measurements are given by (Leiterer et al. 2005) and by (Miloshevich et al. 2001, 2004).

The response time of the Humicap sensor is increasing exponentially with decreasing temperature ( $\sim 0.5\text{--}1$  s at  $+20^\circ\text{C}$ ;  $\sim 2\text{--}8$  s at  $-20^\circ\text{C}$ ;  $\sim 60\text{--}200$  s at  $-60^\circ\text{C}$ ), such that vertical structures in atmospheric humidity profiles are increasingly smoothed with decreasing temperature (i.e. increasing altitude). Vertical RH-profiles may be corrected for this time-lag effect by applying algorithms developed by (Miloshevich et al. 2004). A time lag correction will reduce the measurement uncertainty for individual profiles, increase the significance in larger data sets, and may reduce systematic biases in regions of the atmosphere, where the vertical RH gradient has a climatological preference.

For RS80-sondes manufactured before June 2000 outgassing of packaging material contaminated the Humicap sensors causing a dry bias of 2% and 10% of measured RH for 1-yr old RS80-A and RS80-H sondes, respectively. For RS90 and RS92 daytime measurements solar radiation can be the dominant systematic error source causing a dry bias, however, this can be corrected for.

After correction of all identified systematic biases and time lag effects Vaisala radiosondes may measure relative humidity with a relative uncertainty of about  $\pm(3\text{--}5)\%$  at ambient temperatures above  $-20^\circ\text{C}$  for RS80-A/H and RS90/92 radiosondes. However, at lower temperatures the relative uncertainty is increasing to  $\pm 10\%$  for RS80-A and  $\pm(5\text{--}10)\%$  for RS80-H or RS90. RS92 sensors may achieve a relative uncertainty of  $\pm 5.5\%$  for night time observations and  $\pm 6.5\%$  for day time observations (incl.  $\pm 1.5\%$  uncertainty contribution due to production variability), plus an RH-offset uncertainty of  $\pm 0.5\%$  RH (Miloshevich et al. 2009).

**Table 2.1** Factors affecting humidity measurements by the RS80, RS90 and RS92 radiosondes

Factor	RS80-A	RS80-H	RS90	RS92
Batch variation in basic calibration at room temperature	Yes	Yes	No (direct multi point calibration against references)	No
Calibration model error (mainly at low temperatures)	Yes (large, due to linear model, last change in 1985)	Yes (smaller, TD correction model improved since 1990)	Yes (improved May 2001)	Yes (improved April 2004)
Chemical contamination of sensor	Yes (corrected by using drying agent in September 1998 and a protection shield in May 2000)	Yes (larger than for the RS80-A, corrected by using drying agent in September 1998 and a protection shield in May 2000)	Yes (minimized)	No (corrected by using reconditioning cycle in ground check unit)
Sensor wetting or icing	Yes	Yes	Yes (minimized by heated twin sensor)	Yes (minimized by heated twin sensor and extended heating cycles)
Humidity time lag (at cold)	Yes	Yes (larger than RS80-A)	Yes (smaller than RS80-A)	Yes (smaller than RS80-A)
Solar radiation heatings	Yes	Yes	Yes (larger than RS80)	Yes (larger than RS80)



**Fig. 2.4** Airbus A340 equipped with MOZAIC-humidity device. Inlet system is mounted at the outside skin of the aircraft close to the cone

To reduce the estimated uncertainties of operational radiosondes as well as for reference instruments large efforts have been started in the scope of the Global Climate Observing System (GCOS) Reference Upper Air Network (GRUAN), (Seidel et al. 2009) as well the development of a new humidity sensor for balloon borne radiosonde measurements (Vaisala et al. 2010).

## 2.3 Humidity Monitoring from Aboard Commercial Aircraft: MOZAIC-Program

### 2.3.1 Introduction to MOZAIC-Program

MOZAIC (Measurements of ozone and water vapour by Airbus in-service aircraft) is an European project funded by the European Union for the measurement of the large scale distribution of trace gases like ozone, water vapour, nitrogen oxides and carbon monoxide from board of commercial Airbus A340-aircraft (Fig. 2.4) during scheduled “in-service” flights (Marenco et al. 1998), <http://mozaic.aero.obs-mip.fr/web/>.

Since 1994 compact light weighted humidity devices are flown on five A340-aircraft operated by several European airlines (Lufthansa: 2 aircraft; Air France, Austrian Airlines and Sabena each 1 aircraft). The MOZAIC-flight routes cover a large extent of the northern hemisphere and parts of the southern hemisphere (Fig. 2.5). Every flight includes vertical profiles during takeoff/landing and continuous data at cruise altitude. Particularly the recording at cruise altitude between 9 and



**Fig. 2.5** Overview of major flight routes with MOZAIC humidity measurements since August 1994. The numbers give the percentage of individual flight routes out of all flight

12 km altitude covers large areas of the upper troposphere and lower stratosphere, an important region with the largest climate sensitivity. Data from more than 25000 flights (comprised of two vertical profiles and about 8 hours of data in the UTLS per flight) have been collected since 1994. The data are stored in a scientific data base at CNRM (Toulouse, France) (<http://mozaic.aero.obs-mip.fr/web>).

Presently, three of the MOZAIC-aircraft (2 Lufthansa and 1 Air Namibia) are still in service. However, MOZAIC is entering a new phase as part of the IAGOS (In-service Aircraft for a Global Observing System) project (<http://www.iagos.org/>). IAGOS aims to fly instruments on a larger fleet of about 20 aircraft with a long term mission over the next 10–20 years and a better global coverage in both hemispheres. The first two IAGOS aircraft have started their mission in 2011 and 2012, respectively.

### 2.3.2 MOZAIC Humidity Device (MHD)

Relative humidity and temperature are measured with a compact airborne sensing device AD-FS2 (Aerodata, Braunschweig, Germany), as shown in Fig. 2.6 and described in detail by (Helten et al. 1998). The sensing element consists of a capacitive sensor (Industrial version Humicap-H, Vaisala, Finland) with a hydroactive polymer film as dielectric whose capacitance depends on the relative humidity (Anderson et al. 1995) plus a platinum resistance sensor (PT100) for the direct measurement of the temperature at the humidity sensing surface. The humidity and temperature signals are linearized by a microprocessor controlled transmitter unit (HMP-230, Vaisala, Finland), which passes the relative humidity (RH) and the temperature signal to the automated data acquisition system of MOZAIC located in the avionic bay of the aircraft (Marenco et al. 1998). The humidity sensing element, together with

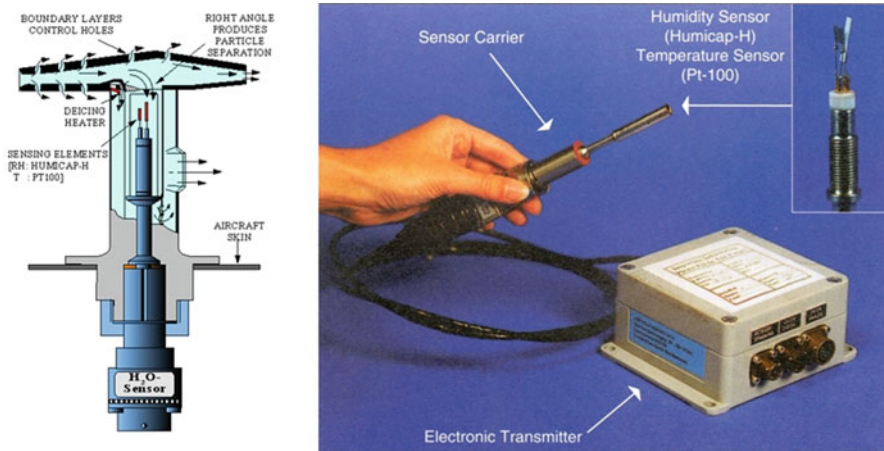


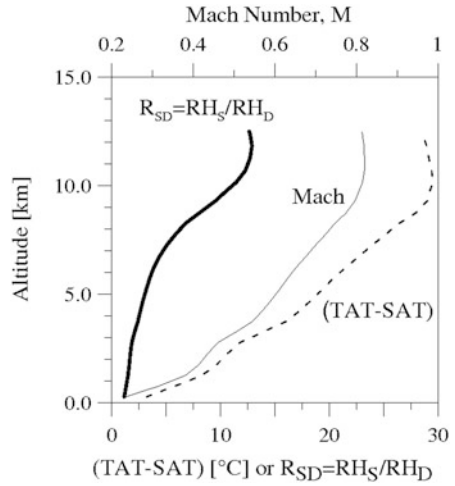
**Fig. 2.6** Left panel: Cross section of the airborne MOZAIC humidity sensor mounted in air sampling housing (Rosemount, Model 102 BX). Right panel: MOZAIC Humidity Device (MHD) consisting of the sensor carrier (including sensing element of Humicap-H and Pt100) to be installed in the Rosemount housing mounted on the outside skin of the Airbus A340 aircraft (Fig. 2.4) and a microprocessor-controlled transmitter unit ( $H \times L \times W = 120 \times 180 \times 130$  mm, Total weight  $\sim 1.5$  kg, Power consumption 5 VA at 28 VDC)

the PT100-resistor, are mounted at the top of an axisymmetric body, which is designed for installation in an appropriate housing (Model 102 BX, Rosemount Inc., Aerospace Division, USA). The sensor housing (Fig. 2.6) is known to derive accurate ambient air temperatures (Stickney et al. 1994).

The housing with both sensors is positioned outside the fuselage, 7 m backwards from the aircraft nose on the left side just below the cockpit. Air sampling occurs at a distance of 7 cm from the aircraft skin, well outside the local boundary layer (thickness only 3 cm) of the aircraft, thus avoiding contaminating interferences that might originate from the aircraft skin. The sampled air flow is divided into two sub flows inside the inlet of the housing. The main flow traverses straight through the housing. The minor flow makes a sharp right angle turn to a smaller channel, perpendicular to the main channel, passing over the sensor elements before reaching a small outlet, located at the lower back side of the housing. The right angle turn of the secondary air flow protects the sensors against dust, hydrometeors and particles. The internal boundary layer air is sucked off through small holes in the side walls of the housing, minimising internal boundary-layer effects. This protects the core of the sampled air flow from thermal or humidity influences as might originate from contact of the outer parts of the sampled flow with the walls of the housing.

The air entering the Rosemount housing is subject to adiabatic compression caused by the strong speed reduction in the inlet part of the housing. The conversion of the kinetic energy of the sampled air into heat leads to a significant temperature increase of the air sampled by the sensor. The thermal recovery process at the sensing element is well defined (Stickney et al. 1994). In flight, Static Air Temperature (SAT) is the

**Fig. 2.7** Mean values of the speed of the MOZAIC aircraft (Mach number, *thin solid line, upper scale*) as a function of altitude. The *broken line (lower scale)* gives the corresponding difference between the temperature measured by the sensor and the ambient temperature (*TAT-SAT*) and the *thick solid line* gives the ratio between ambient and measured relative humidity ( $RH_S/RH_D$ )



temperature of the undisturbed air through which is about to fly. Total Air Temperature (*TAT*) is the maximum temperature that can be attained by 100 % conversion of the kinetic energy into heat of the air sample. The relation between total and static air temperature is:

$$TAT = SAT \left( 1 + \left( \frac{c_p - c_v}{2c_v} \right) M^2 \right) \quad (2.2)$$

In Eq. 2.2,  $c_p$  and  $c_v$  are the specific heats of dry air at constant pressure and volume, respectively, and  $M$  is the Mach number, i.e. ratio of the aircraft speed (relative to air) relative to the speed of sound.  $M$  is available in flight from the avionic system of the aircraft.  $M$  typically increases from values of about 0.2 near ground to  $0.81 \pm 0.01$  at cruise altitude (Fig. 2.7). The conversion of kinetic energy inside the housing is not exactly 100 %. Therefore, the temperature measured by PT100 inside the housing, the total recovery temperature (*TRT*), is lower than the total air temperature (*TAT*), expected after a complete conversion of the kinetic energy. The housing manufacturer provides an empirical recovery factor  $\eta$  to determine the real *TAT* from *TRT* by the relation

$$TAT = \frac{TRT}{1 - \eta} \quad (2.3)$$

The recovery factor  $\eta$ , determined from a series of wind channel experiments, is a function of the Mach number and given by a function table (Stickney et al. 1994). Even at large Mach numbers the recovery factor is smaller than 0.004 such that corrections of *TRT* to *TAT* are always smaller than 1 K.

The adiabatic compression produces an appreciable temperature rise relative to the ambient static air temperature (*SAT*) if the aircraft speed is comparable to the speed of sound (Fig. 2.7). The resulting difference between total and static air temperature (*TAT-SAT*) increases from 2 K near ground to approximately 30 K at 10–12 km cruise

altitude. Because of the strong temperature increase, the relative humidity  $RH_D$  detected by the sensing element in the Rosemount housing is appreciably lower than the static relative humidity of the ambient air,  $RH_S$  (Helten et al. 1998).

$$RH_S = RH_D \left( \frac{SAT}{TAT} \right)^{\frac{c_p}{c_p - c_v}} \frac{E_W(TRT)}{E_W(SAT)} \quad (2.4)$$

The first factor in Eq. 2.4 describes the adiabatic compression, while the second term accounts for the different water vapour saturation pressures  $E_W$  at  $SAT$  and  $TRT$ , respectively.

For the evaluation of the water vapour data we follow the formulation of  $E_W$  by (Goff and Gratch 1946) over a plane surface of pure liquid water, as recommended by the World Meteorological Organisation (WMO 1983) and adapted to the International Temperature Scale 1990 (ITS-90; Sonntag 1994):

$$E_W(T) = \exp \left( \frac{a}{T} + b + c \cdot T + d \cdot T^2 + e \cdot \ln(T) \right) \quad (2.5)$$

where  $E_W$  is in Pa and  $T$  in K. For a liquid water surface, the constants are:  $a = -6096.9385$  K,  $b = 21.2409642$ ,  $c = -2.711193 \times 10^{-2} \text{ K}^{-1}$ ,  $d = 1.673952 \times 10^{-5} \text{ K}^{-2}$ ,  $e = 2.433502$ .

At cruise altitude,  $RH_D$  is a factor of 12–13 lower than  $RH_S$  (Fig. 2.7). Therefore, the humidity sensor usually works within the lowest 10 % of its dynamic range. This fact is not adequately covered by the factory calibration provided with the transmitter unit and hence requires regular individual recalibration of each sensor, in particular of the sensor bias.

### 2.3.3 Pre- and Post-Flight Calibration in Environmental Simulation Chamber

Each MOZAIC humidity sensor that is used for the MOZAIC project is individually calibrated in the laboratory at Jülich before installation in the aircraft and again after 500 flight hour intervals. Prior to a preflight calibration the sensor is rinsed with ethanol and then reformed by heating it to 130 °C. Postflight calibrations are done without prior cleaning. The laboratory calibration is executed in an environmental simulation chamber (Fig. 2.8; <http://www2.fz-juelich.de/icg/icg-2/esf>). The chamber is a stainless steel vacuum chamber with a volume of 500 l (80 × 80 × 80 cm) (Smit et al. 2000). Pressure, temperature, and relative humidity are computer controlled to simulate atmospheric flight conditions, which are typically encountered in the troposphere, including tropopause, and lower stratosphere. Typical tropospheric conditions of water vapour concentrations, temperatures, and pressures up to altitudes of 15 km can be simulated. Frost point temperatures down to −80 °C can be reached.

A Lyman( $\alpha$ ) fluorescence hygrometer (Kley and Stone 1978) is installed in the simulation chamber as reference instrument for the measurement of low water vapour

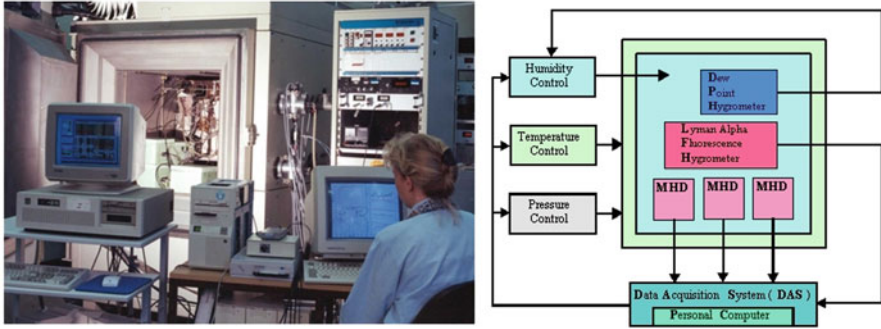


**Fig. 2.8** Environmental simulation facility at Forschungszentrum Juelich (IEK-8) to calibrate MOZAIK-Humidity Devices at typical pressure, temperature and humidity conditions encountered during flight

mixing ratios (1–1000 ppmv) with a relative accuracy of  $\pm 4\%$  (Helten et al. 1998). At water vapour mixing ratios above 1000 ppmv serves a dew/frost point hygrometer (General Eastern, Type D1311R) with an accuracy of  $\pm 0.5$  K. Up to three water vapour sensors can be simultaneously calibrated. They are positioned in the outlet duct flow of the Lyman( $\alpha$ ) hygrometer and sample the air just after it has passed the hygrometer.

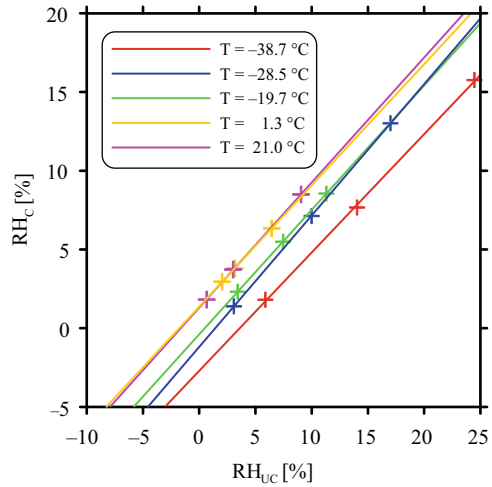
The calibrations revealed that the relative humidity of a calibrated sensor ( $RH_C$ ) for a constant temperature can be expressed by a linear relation

$$RH_C = a + b \cdot RH_{UC} \quad (2.6)$$

where  $RH_{UC}$  is the uncalibrated output from an individual sensor, while the offset ( $a$ ) and slope ( $b$ ) are determined as a function of temperature (Helten et al. 1998). At a fixed sensor temperature, three different levels of humidity are set which correspond to typical conditions encountered at the sensing element during in-flight operation in the troposphere.

To derive the coefficients  $a$  and  $b$  as function of temperature calibrations were executed at three temperatures,  $-20^\circ\text{C}$ ,  $-30^\circ\text{C}$ , and  $-40^\circ\text{C}$  while at higher temperatures an interpolation between the chamber calibration at  $-20^\circ\text{C}$  and the nominal calibration of the manufacturer at  $20^\circ\text{C}$  has been applied (Helten et al. 1998). However, since 1999 additional calibrations at  $0^\circ\text{C}$  and  $20^\circ\text{C}$  have become standard in the calibration process to improve the accuracy of the measurements made in the corresponding altitude region between 0 and 5 km (Fig. 2.9). The pressure at  $-40^\circ\text{C}$  and  $-30^\circ\text{C}$  is set to 180 hPa and increased to 400 hPa at higher temperatures. From investigations made at constant temperature but at different pressures between 100 and 1000 hPa, no significant pressure dependence of the sensitivity of the humidity sensor had been observed (Helten et al. 1998).

**Fig. 2.9** Calibration of a MOZAIC humidity sensor at 5 temperature levels: Reference hygrometer (Lyman Alpha & Dew/Frost point) as a function of the sensor measurement (*crosses*) together with corresponding linear regression fits



### 2.3.4 Assessment of In-Flight Uncertainties

It is recalled that the analysis of the MOZAIC measurement is performed with the averages of the individual preflight and postflight calibration coefficients  $a$  and  $b$  for each interval of 500 hours of flight operation.  $RH_S$  of the ambient air is determined from the measured  $RH_D$ ,  $TRT$ ,  $TAT$ , and  $SAT$  by Eq. 2.4. The uncertainty of  $RH_S$  is deduced by the law of error propagation with the uncertainty of these parameters. The uncertainty of  $RH_D$  is a composite of the following contributions: uncertainty of the Lyman- $\alpha$  hygrometer calibration and half of the absolute value of the differences of the individual preflight and postflight calibration coefficients,  $a$  and  $b$ . To convert to the uncertainty of  $RH_S$ , the uncertainties of  $TAT$  and  $TRT$  (equal to  $\pm 0.25$  °C) and  $SAT$  (equal to  $\pm 0.5$  °C) have to be included. The contribution of uncertainty of the air speed measurement by the aircraft to the uncertainty of temperature determination is below  $\pm 0.01$  °C and was excluded from the error propagation determination. The uncertainty of the recovery factor  $\eta$  of the Rosemount probe housing contributes to the uncertainties of the temperature measurements and, thus,  $RH_S$  recovery. One determines then the total uncertainty of  $RH_S$ . The analysis show that the major contribution comes from the differences of calibration coefficients  $a$  and  $b$  between preflight and postflight calibration (Helten et al. 1998). If these differences are small, then this contribution is of the same order of magnitude as the uncertainty caused by the temperature uncertainty. The MOZAIC database contains estimates of the total uncertainty of  $RH_S$  for each individual humidity data point based on the pre- and post-flight calibration of the flown humidity sensor.

The mean of the pre- and post-flight calibration coefficients of each flight period are used to evaluate the average uncertainty of the measurements. The differences between both sets of these calibration coefficients give the main contribution to the uncertainty of the measurement (Helten et al. 1998). The variations of the uncertainties

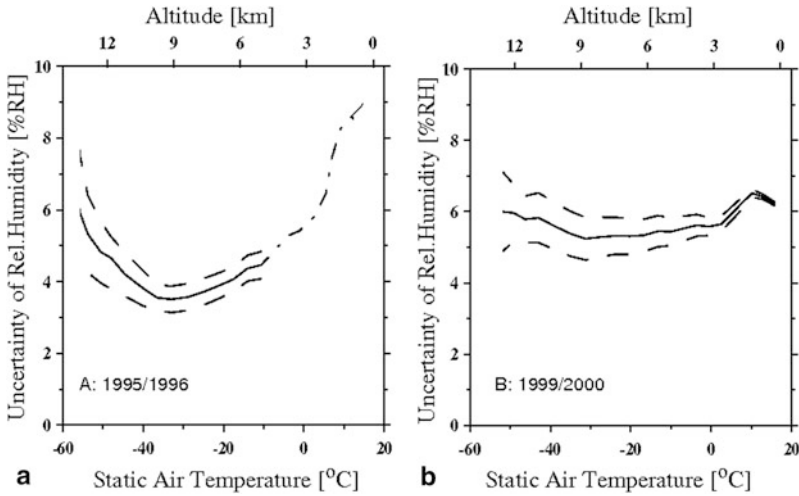


**Fig. 2.10** Mean uncertainty in percent  $RH$  of all MOZAIC relative humidity measurements (*solid curve*) as a function of static air temperature (bottom x-axis) made over 1995 & 1996 (left diagram **a**; calibration at  $-20^{\circ}\text{C}$ ,  $-30^{\circ}\text{C}$ , and  $-40^{\circ}\text{C}$ ) and 1999 & 2000 (right diagram **b**; calibration including  $0^{\circ}\text{C}$  and  $20^{\circ}\text{C}$ ). The standard deviation of the mean is marked by the *dashed curves*. For 1995/1996 (**a**) the region not covered by preflight and postflight calibrations (lower troposphere, see text) is indicated with an estimated mean uncertainty (*dashed/dotted line*). The corresponding altitude is indicated as the top x-axis

of the  $RH$  measurements were determined as the mean of all individual total uncertainties over all MOZAIC data as a function of SAT for 1996/1997 and 1999/2000, representative for calibrations made at the three lower temperatures ( $-20^{\circ}\text{C}$ ,  $-30^{\circ}\text{C}$ , and  $-40^{\circ}\text{C}$ ) and inclusion of higher temperatures ( $0^{\circ}\text{C}$  and  $20^{\circ}\text{C}$ ), respectively (Fig. 2.10). The standard deviation is also shown. For 1994–1998 data (left diagram) the uncertainty ranges from  $\pm 7\%$   $RH$  at  $-55^{\circ}\text{C}$  ( $\approx 13$  km) down to  $\pm 4\%$   $RH$  at  $-40^{\circ}\text{C}$  ( $\approx 10$  km). At lower altitude, for SAT ranging between  $-40^{\circ}\text{C}$  ( $\approx 9$  km) and  $-20^{\circ}\text{C}$  ( $\approx 6$  km) the uncertainty is within  $\pm(4-6)\%$   $RH$ , increasing above  $0^{\circ}\text{C}$  (near ground level) to  $\pm 8\%$   $RH$ . For the region below 5 km altitude, only an interpolation between the sensor calibration made in the chamber at  $-20^{\circ}\text{C}$  and the nominal calibration of the sensor manufacturer is used, indicated as a dashed dotted line in Fig. 2.10. However, since 1999 after inclusion of sensor calibration at  $0^{\circ}\text{C}$  and  $20^{\circ}\text{C}$  the accuracy below 5 km has increased significantly. From the regular pre- and post-flight calibration of each flown sensor typical  $1\sigma$ -uncertainties of  $\pm(4-6)\%$  relative humidity between surface and 12 km altitude are obtained. It is to be noticed that the relative uncertainties of the measurements are rapidly increasing in dry air. For measurements of stratospheric humidity, where relative humidities well below 5% prevail, the uncertainty of the MOZAIC humidity device is insufficient for quantitative water vapour measurements.

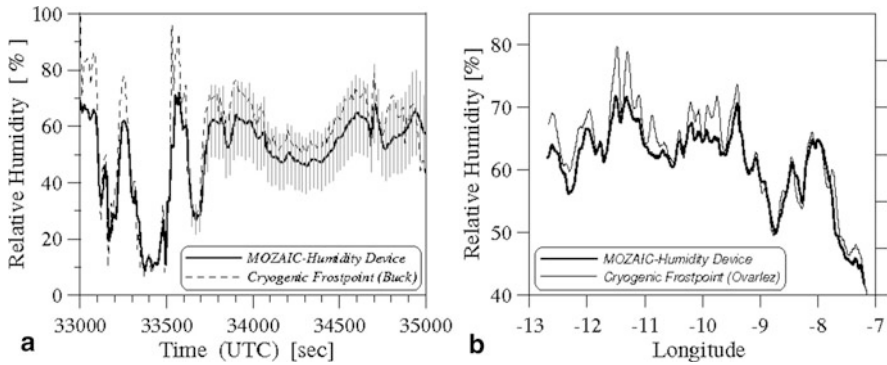


**Fig. 2.11** (a) Relative humidity measured by MHD and cryogenic frostpoint hygrometer (Busen and Buck 1995) as function of flight time during intercomparison flight on board the DLR Falcon aircraft in March 1995 (Helten et al. 1998). (b) Relative humidity measured by MHD on the MOZAIC-Airbus aircraft and cryogenic frostpoint hygrometer (Ovarlez and Velthoven 1997) on the DLR Falcon aircraft as a function of longitude during a dedicated comparison flight in September 1997. The Falcon followed the Airbus at a distance of 7 to 35 km. (Source: Helten et al. 1999)

### 2.3.5 *In-Flight Comparison of MHD With Other Hygrometer: Time Response and Spatial Resolution*

The in-flight performance of the MOZAIC-humidity device had been assessed by intercomparison with reference instrumentation during dedicated research aircraft missions. Fig. 2.11 shows results from two missions with a Fanjet Falcon E research aircraft of the Deutsches Zentrum für Luft- und Raumfahrt (DLR), the in-flight performance of the MHD was assessed by intercomparison with reference instrumentation. The first in-flight comparison of the MHD against reference instrumentation was conducted in 1995 with the MHD mounted aboard the Falcon aircraft (Helten et al. 1998). As reference served an airborne cryogenic frostpoint hygrometer, with a relative accuracy of  $\pm 10\%$  (Busen and Buck 1995). The second mission took place in 1997 whereby the Falcon aircraft approached the flight path of the MOZAIC-aircraft at  $13^\circ$  W longitude and followed until  $7^\circ$  W longitude (Helten et al. 1999). The Falcon aircraft was equipped with a cryogenic frostpoint hygrometer developed for airborne water vapour mixing ratio measurements with a relative accuracy of about  $5\%$  (Ovarlez and van Velthoven 1997). Both aircraft missions confirmed the results yielded from pre- and post-flight calibrations (Helten et al. 1998). Similar results (Fig. 2.12) were obtained more recently in 2006 during an in-flight comparison of the MHD with the Jülich Lyman- $\alpha$  fluorescence hygrometer, FISH (relative accuracy  $\pm 5\%$ ; (Zöger et al. 1999) made from aboard a Learjet 35 aircraft (Kunz et al. 2008).

The structures measured with the reference instruments are smoothed by the MHD. This is caused by the response time of the MHD which increases with decreasing sensor temperature due to the adsorption and diffusion of water molecules into the

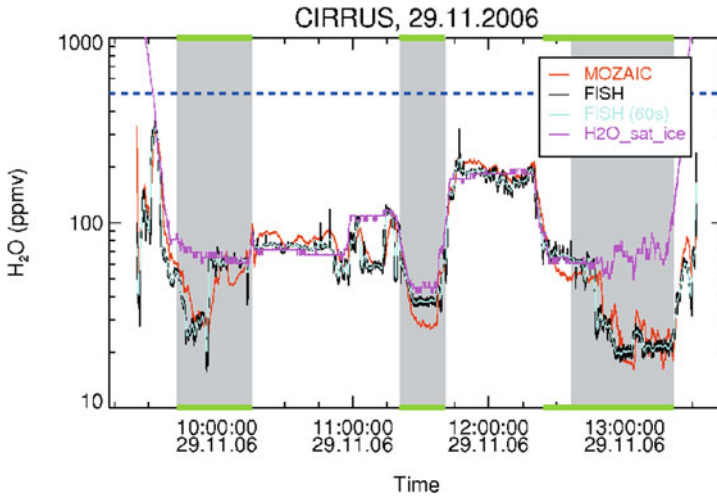


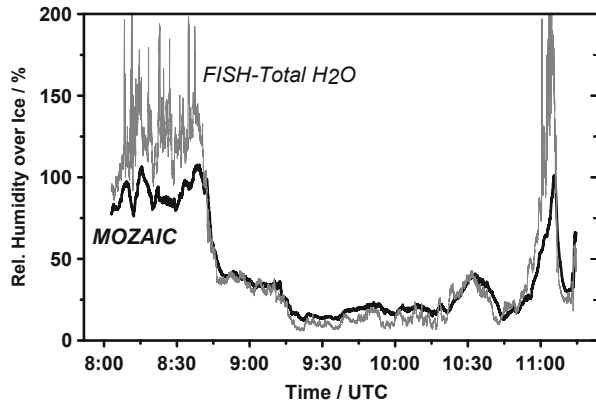
**Fig. 2.12** In-flight comparison of water vapour mixing ratio measured by MHD and FISH as function of flight time during one flight mission on board the Learjet 35 A aircraft in November 2006. (Source: Kunz et al. 2008)

sensor material (Antikainen and Paukkunen 1994). It is inferred from Fig. 2.11 that at sensor temperatures (equal to  $TRT$ ) of about  $-30^{\circ}\text{C}$  the response time is several minutes. Above  $-10^{\circ}\text{C}$  the MHD tracks fine structures in the humidity field well, but measures drier values compared to the frost point hygrometer. This is most likely due to the fact that before 1999 the MOZAIC sensor was not calibrated at these relative high sensor temperatures. The response time of the MOZAIC sensor during ascent and descent is well below 10 s near ground and below 1 min around 9 km altitude (Helten et al. 1998). This means that at an ascent/descent rate of the MOZAIC aircraft of about 8 m/s, the vertical resolution of measured vertical humidity profiles is better than 100 m in the lower troposphere and around 500 m in the upper troposphere. At cruise altitude the response time is about 1–3 min such that at a horizontal aircraft speed of 250 m/s, the horizontal resolution is about 15–50 km which is sufficient to record large-scale distributions of upper tropospheric water vapour.

### 2.3.6 Performance at High Relative Humidities: Ice Super Saturation

In the upper troposphere ( $Z=9-12$  km) a substantial fraction (0.1–0.3) of the MOZAIC-relative humidity measurements show supersaturation with respect to ice (e.g. Gierens et al. 2000; Luo et al. 2007). A common phenomena common observed from other measurement platforms in the upper troposphere, both in clear and cloudy regions (e.g. Heymsfield et al. 1998; Jensen et al. 1998; Vay et al. 2000; Comstock

**Fig. 2.13** In-flight comparison of relative humidity with respect to ice measured by MHD (*thick black*) and FISH-Total H<sub>2</sub>O (*thin grey*) as function of flight time during a research flight on board the Learjet 35 A aircraft in April 2003. Cruise altitude 11–12 km and air temperature 215–220 K

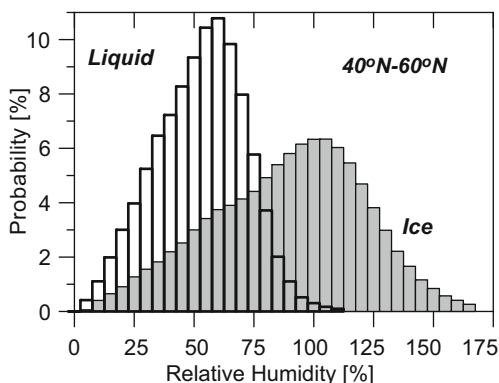


et al. 2004). An important feature suggesting that water vapour in the upper troposphere is for a significant fraction of time not in thermodynamical equilibrium with the ice phase. However, in how far these *RH* measurements are artifacts (e.g. evaporation of ice crystals in inlet system due to adiabatic heating) or real atmospheric features? At low temperatures it is very unlikely that the contamination of evaporating ice crystals is a significant error source for the following reasons:

1. In wind tunnel experiments with true air speed (*TAS*)  $\sim 100$  m/s it was shown that only particles smaller than  $1 \mu\text{m}$  have a considerably high chance to get to the *RH*-sensing element in the Rosemount housing (O. Reynolds, UK Met Office, 2003, personal communication). However, the *TAS* in real flights is rather  $\sim 250$  m/s, thus reducing additionally the probability of incoming ice crystals. These small ice crystals have masses on the order of  $10^{-15}$  kg and for usual ice crystal number concentrations ( $N < 10 \text{ cm}^{-3}$ ) the net effect is probably negligible.
2. In situ comparisons of the MHD with the FISH-total water vapour instrument (Schiller et al. 2008) on board a Learjet 35A aircraft show no evidence of contamination of the gas phase water vapour measurement of MOZAIC inside cirrus (Fig. 2.13). Below ice saturation the MHD tracks the FISH very well. However, at saturation levels above 100 % *RH* with respect to ice the behavior of both instruments is very different. Although the MHD stays close to 100 % *RH* with respect to ice, the FISH detects excesses of water vapour because it measures total water vapour, i.e. gaseous phase plus contribution of liquid/ice phase which has been forced to evaporate by heating before detection.
3. Only a very small fraction of 0.5 % of all MOZAIC measurements (complete data base) show *RH* values in excess of 100 % with respect to liquid water, whereas more than 30 % of the data in the tropopause region show ice supersaturation (Fig. 2.14). In case of massive contamination due to evaporating ice crystals the frequency of occurrence for *RH* > 100 % “values” should be enhanced.

In the lower and middle troposphere at warmer temperatures, relative humidity values in excess of 100 % to liquid water are occasionally observed. This contamination is

**Fig. 2.14** Probability distribution function of relative humidity with respect to liquid water (*thick black*) and ice (*thin black, grey shaded area*) in UT between 40°–60° N obtained over the Atlantic (10°–70° W) over more than 1000 flights made in 1998



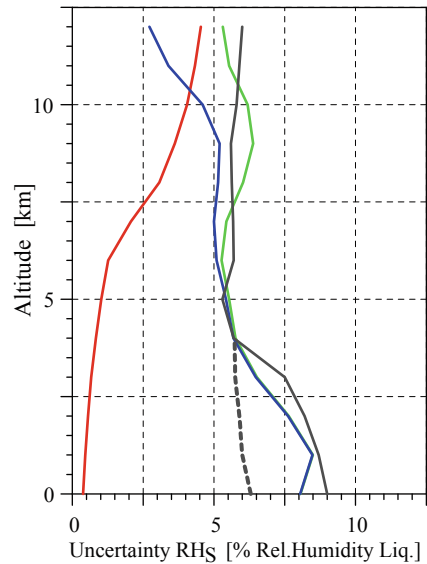
most likely caused by partial or complete evaporation of liquid droplets after entering the Rosemount inlet. In contrast to ice particles, the strong shear flow forces caused by the strong speed reduction, can atomize liquid droplets into a large number of very small droplets that evaporize much faster than ice particles with the same water content.

### 2.3.7 *New Developments: In-Flight Calibration Method*

While MOZAIC has demonstrated the large potential of in-service aircraft as a cost efficient platform for obtaining high quality humidity data in the free and upper troposphere, a larger fleet of aircraft is required for obtaining a truly global picture. This calls for a measurement system that is (i) compact, light-weight, and quasi maintenance-free and (ii) reliable, precise, and sufficiently accurate. The MOZAIC humidity sensor has shown to fulfill these criteria (Kley et al. 2000). However, the method of pre- and post-flight calibration in the laboratory every 500 hours of operation, as applied in MOZAIC, is not suitable for real-time data provision, a pre-requisite for operational use in meteorological networks. Therefore, based on the experience gained on instrument characteristics at different temperatures during 10 years of MOZAIC-operation a novel method for automatic in-flight calibration (IFC) of the sensors has been developed and described in detail by (Smit et al. 2008).

The IFC method corrects the potential drift of the sensor offset at zero relative humidity, which is the critical parameter in determining the uncertainty of the measurements. Any drift of the sensor offset is caused by additional bonding of non-water molecules originated from polluted air. However, praxis has shown that the offset drifts slowly and only significant changes have been first observed after 4–8 weeks of flight operation. The sensor offset is determined from the measurements themselves as obtained during periods when the aircraft is flying in the lower stratosphere at or above the hygropause where the H<sub>2</sub>O mixing ratio reaches well defined minimum values of about 5 ppmv and the contribution of atmospheric H<sub>2</sub>O to the sensor signal

**Fig. 2.15** Total uncertainty of the relative humidity profile (green curve) calculated from the uncertainty of the average slope  $b$  (blue curve) and the uncertainty of the offset  $a$  (red curve) obtained from the IFC-method. For comparison, the average uncertainty of the MOZAIC calibrations is also shown (black solid curve: based on calibrations between 235 K and 260 K as reported by (Helten et al. 1998); dashed black curve: valid since 1999, after extending the calibrations at sensor temperatures of 270–290 K. (Source: Smit et al. 2008))



is minimal. The selection of stratospheric data is achieved with the help of potential temperature that can be calculated in-situ from measured temperature and pressure.

The IFC method is capable of providing humidity measurements in near real time with an uncertainty of  $\pm 8\% RH$  at the surface and  $\pm 7\% RH$  in the upper troposphere (Fig. 2.15). For validation, the IFC method was applied to five years of archived raw signals from the MOZAIC aircraft. The resulting humidity data are in good agreement (within  $2\% RH$ ) with the original MOZAIC data that used monthly pre- and post flight calibrations of the sensor. The standard deviation of the differences varies with altitude between  $\pm 4\%$  and  $\pm 6\% RH$  which is comparable to the accuracy of the MOZAIC laboratory calibrations (Fig. 2.15).

At the typical cruise altitude of longhaul aircraft (9–12 km), the IFC method is most efficient and accurate at higher latitudes where dry stratospheric air coincides with relatively high ambient temperatures (220–230 K), hence providing the lowest contribution to the signal of the sensor, which measures relative humidity. At these conditions the a priori assumption of 5 ppmv for the water vapour mixing ratio at the hygro-pause is not critical for the accuracy of the method. Compared to MOZAIC-operation based on monthly calibrations in the laboratory the use of IFC will substantially reduce the efforts for maintenance and thus will enable to operate the sensor on a large fleet of in-service aircraft for near real time measurements of humidity in the troposphere. The IFC method will not work, however, on aircraft that never enter the lower stratosphere, e.g. aircraft that fly exclusively regional routes or in the tropics. Regular offline calibrations will remain important for such aircraft.

### 2.3.8 Summary and Conclusions

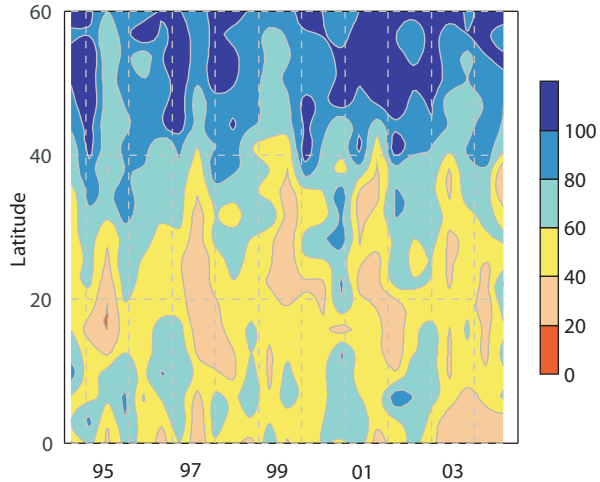
The MOZAIC project features more than 15 years of continuous measurements of water vapour from board commercial Airbus A340 aircraft during scheduled flights. Thereby capacitive humidity sensing devices are used to measure tropospheric relative humidity together with temperature from aboard aircraft, if the sensors are carefully calibrated before their installation and after deinstallation. After an operation time of 4–6 weeks (~500 flight hours) the differences between preflight and postflight calibration result in uncertainties  $\pm(4-6) \% RH$  for measurements between surface and 12 km altitude. For dry regions with low relative humidities (e.g. stratosphere) the uncertainty of  $\pm(4-6) \% RH$  is getting limited for accurate humidity measurements.

The installation of the humidity sensor in an appropriate housing (Rosemount Model 102 BX), normally used in aviation to measure accurate ambient air temperature, has the advantage of protection against the impact of particles or dust. Also, wall contact of the sampled air, which would influence temperature and humidity, is avoided. Adiabatic compression causing a temperature increase of the sampled air leads to a reduction of the dynamic range of the sensor, but also provides for sufficient time response at low static air temperatures. There are no indications that MOZAIC-observations of ice super saturation in the upper troposphere are interfered by evaporation of ice crystals in the Rosemount inlet. In the lower and middle troposphere at higher temperatures in the presence of liquid droplets contamination from evaporation can occur because at the inlet droplets might atomize into a large number of very small droplets which evaporate much faster.

In-flight intercomparisons with a Lyman- $\alpha$  fluorescence hygrometer and a frost point hygrometer showed good agreement within  $\pm(5-10) \% RH$  for measurements in the middle/upper troposphere. The deviations of the Humicap sensor observed during this in-flight intercomparison is in agreement with the uncertainty obtained from the estimated overall uncertainty which is dominated by contribution of the differences observed between preflight and postflight calibrations. The time response of the sensor in the lower/middle troposphere is good, but increases at lower temperatures to values of about 1 min at cruise altitude. Vertical resolution of humidity profiling during ascent and descent of the MOZAIC aircraft is better than 100 m in the lower part of the profile and around 200 m in the upper part of the profile. At cruise altitude the horizontal resolution of humidity measurements is around 15 km which is sufficient for climatological purposes.

A new method for in-flight calibration (IFC) has been developed, whereby the sensor offset is quasi-continuously monitored and adjusted in flight, while the less critical sensor sensitivity can be determined at longer (yearly) intervals. Through the use of the IFC-method the sensor needs only to be recalibrated on much longer time intervals (yearly) compared to the monthly calibrations as applied in MOZAIC. This enables operating the sensors on a larger fleet of aircraft with about the same amount of calibration efforts. Consequently, the IFC method will reduce maintenance drastically that make the sensor a serious candidate for real time humidity measurements

**Fig. 2.16** 10 year climatology of the latitudinal (averaged over 10–70°W longitude) distribution of upper tropospheric relative humidity (in % with respect to ice) obtained from MOZAIC-measurements between August 1994 and December 2004



in synoptical networks for weather forecasting. The IFC method is capable of providing humidity measurements in near real time with an uncertainty of  $\pm 8\%$  RH at the surface and  $\pm 7\%$  RH in the upper troposphere.

MOZAIC has demonstrated the large potential of in-service aircraft as a cost efficient platform for obtaining high quality humidity data in the free and upper troposphere. MOZAIC has provided the first measured climatology of upper tropospheric humidity. The observations showed that the UT at cruise altitude (9–12 km) is much more wet than has been assumed before (Fig. 2.16) and that 15–30% of the UT is ice super-saturated (relative humidity in excess of 100% with respect to ice) (Gierens et al. 2000). However, to obtain a truly global picture the measurements will be expanded on larger fleet of aircraft in the scope of the IAGOS (In-service Aircraft in a Global Observing System).

## References

- P.S. Anderson, Mechanism for the behaviour of hydroactive materials used in humidity sensors. *J. Atmos. Ocean. Tech.* **12**, 662–667 (1995)
- V. Antikainen, A. Paukkunen, Dies on improving humidity measurements in radiosondes, in instruments and observing methods. *Tech. Rep.* **57** (1994), WMO, Geneva
- R. Busen, A. Buck, A high-performance hygrometer for aircraft use: Description, installation, and flight data. *J. Atmos. Ocean. Tech.* **12**, 73–84 (1995)
- K.E. Cady-Pereira, M.W. Shephard, D.D. Turner, E.J. Mlawer, S.A. Clough, T.J. Wagner, Improved daytime column-integrated precipitable water vapor from Vaisala radiosonde humidity sensors. *J. Atmos. Ocean. Tech.* **25**, 873–883 (2008)
- P.E. Ciesielski, R.H. Johnson, J. Wang, Correction of humidity biases in Vaisala RS80-H Sondes during NAME. *J. Atmos. Ocean. Tech.* **26**, 1763–1780 (2009)
- J.M. Comstock, T.P. Ackerman, D.D. Turner, Evidence of high ice supersaturation in cirrus clouds using ARM Raman lidar measurements. *Geophys. Res. Lett.* **31**, L11106 (2004) doi:10.1029/2004GL019705

- K. Gierens, U. Schumann, M. Helten, H. Smit, P. Wang, Ice-supersaturated regions and subvisible cirrus in the northern midlatitude upper troposphere. *J. Geophys. Res.* **105**, 22743–22753 (2000)
- J.A. Goff, S. Gratch, Low-pressure properties of water from –160 to 212 F, in Transactions of the American society of heating and ventilating engineers. Paper presented at the 52nd annual meeting of the American society of heating and ventilating engineers, New York, 95–122, 1946
- J. Gorman, 2002, Evaluation of desiccants, Instrum. test rep. 2002 664, Aust. Bur. of Meteorol., Melbourne, Victoria, Australia, available at [www.wmo.int/pages/prog/www/IMOP/WebPortal-AWS/Tests/ITR664.pdf](http://www.wmo.int/pages/prog/www/IMOP/WebPortal-AWS/Tests/ITR664.pdf)
- M. Helten, H.G.J. Smit, W. Straeter, D. Kley, P. Nedelec, M. Zöger, R. Busen, Calibration and performance of automatic compact instrumentation for the measurement of relative humidity from passenger aircraft. *J. Geophys. Res.* **103**, 25643–25652 (1998)
- M. Helten, H. Smit, D. Kley, J. Ovarlez, H. Schlager, R. Baumann, U. Schumann, P. Nedelec, A. Marengo, In-flight intercomparison of MOZAIC and POLINAT water vapour measurements. *J. Geophys. Res.* **104**, 26087–26096 (1999)
- A.J. Heymsfield, L.M. Miloshevich, C. Twohy, G. Sachse, S. Oltmans, Upper tropospheric relative humidity observations and implications for cirrus ice nucleation. *Geophys. Res. Lett.* **25**, 1343–1346 (1998)
- E. Jensen, O.B. Toon, A. Tabazadeh, G.W. Sachse, B.E. Anderson, K.R. Chan, C.W. Twohy, B. Gandrud, S.M. Aulenbach, A. Heymsfield, J. Hallett, B. Gary, Ice nucleation processes in upper tropospheric wave-clouds observed during SUCCESS. *Geophys. Res. Lett.* **25**, 1363–1366 (1998)
- D. Kley, E. Stone, Measurement of water vapor in the stratosphere by photodissociation with Ly $\alpha$  (1216 Å) light. *Rev. Sci. Instrum.* **49**, 691–874 (1978)
- D. Kley, J.M. Russell III, C. Phillips, SPARC Assessment of upper tropospheric and stratospheric water vapour, SPARC Report 2, SPARC Water Vapour Working Group, 2000
- A. Kunz, C. Schiller, F. Rohrer, H.G.J. Smit, P. Nedelec, N. Spelten, Statistical analysis of water vapour and ozone in the UT/LS observed during SPURT and MOZAIC. *Atmos. Chem. Phys.* **8**, 6603–6615 (2008)
- U. Leiterer, H. Dier, D. Nagel, T. Naebert, D. Althausen, K. Franke, A. Katz, F. Wagner, Correction method for RS80-A Humicap humidity profiles and their validation by lidar backscattering profiles in tropical cirrus clouds. *J. Atmos. Ocean. Tech.* **22**, 18–29 (2005)
- Z. Luo, D. Kley, R.H. Johnson, H. Smit, Ten years of measurements of tropical upper-tropospheric water vapor by MOZAIC. Part I: Climatology, variability, transport, and relation to deep convection. *J. Clim.*, **20**, 418–435 (2007). doi:10.1175/JCLI3997.1
- A. Marengo, V. Thouret, P. Nedelec, H. Smit, M. Helten, D. Kley, F. Karcher, P. Simon, K. Law, J. Pyle, G. Poschmann, R.V. Wrede, C. Hume, T. Cook, Measurement of ozone and water vapour by Airbus in-service aircraft: The MOZAIC airborne program, An Overview. *J. Geophys. Res.* **103**, 25631–25642 (1998)
- M. Matsuguchi, S. Umeda, Y. Dadaoka, Y. Sakai, Characterization of polymers for a 24 capacitive type humidity sensor based on water absorption behavior. *Sensors and Actuators* **49**, 179–185 (1998)
- L.M. Miloshevich, H. Vömel, A. Paukkunen, A. Heymsfield, S.J. Oltmans, Characterization and Correction of relative humidity measurements from Vaisala RS80-A radiosondes at cold temperatures. *J. Atmos. Ocean. Tech.* **18**, 135–156 (2001). doi:10.1175/1520-0426(2001)018h0135:CACORHi2.0.CO; 2
- L.M. Miloshevich, A. Paukkunen, H. Vömel, S.J. Oltmans, Development and validation of a time lag correction for Vaisala radiossnde humidity measurements. *J. Atmos. Ocean. Tech.* **21**, 1305–1327 (2004)
- L.M. Miloshevich, H. Vömel, D.N. Whiteman, B.M. Lesht, F.J. Schmidlin, F. Russo, Absolute accuracy of water vapor measurements from six operational radiossnde types launched during AWEX-G and implications for AIRS validation. *J. Geophys. Res.* **111**, D09S10 (2006). doi:10.1029/2005JD006083

- L.M. Miloshevich, H. Vömel, D.N. Whiteman, T. Leblanc, Accuracy assessment and correction of Vaisala RS92 radiosonde water vapor measurements. *J. Geophys. Res.* **114**, D11305 (2009). doi:10.1029/2008JD011565
- D.M. Murphy, T. Koop, Review of the vapour pressures of ice and supercooled water for atmospheric applications. *Quart. J. Royal Met. Soc* **131**, 1539–1565 (2005)
- H. Nakamura, H. Seko, Y. Shoji, Dry biases of humidity measurements from the Vaisala RS80-A and Meisei RS2-91 radiosondes and from Ground-Based GPS (1. Ground-Based GPS Meteorology). *J. Meteorological Society of Japan. Ser. II*, **82**, 277–299, ISSN 00261165, URL (2004) <http://ci.nii.ac.jp/naid/110001803074/en/>
- J. Nash, R. Smout, T. Oakley, B. Pathack, S. Kurnosenko, WMO Intercomparison of high quality radiosonde systems. Vacoas, Mauritius, 2-25 February 2005. Final report. Tech. rep. (2006) WMO Instruments and Methods of Observation Programme, Geneva, Switzerland
- M. Nuret, J.-P. Lafore, O. Bock, F. Guichard, A. Agusti-Panareda, J.-B. N'gamini, J.-L. Redelsperger, Correction of humidity bias for Vaisala RS80-A sondes during the AMMA 2006 observing period. *J. Atmos. Ocean. Tech.* **25**, 2152–2158 (2008)
- J. Ovarlez, van P. Velthoven, Comparison of water vapor measurements with data retrieved from ECMWF analyses during the POLINAT experiment. *J. Appl. Meteorol.* **36**, 1329–1335 (1997)
- A. Paukkunen, Sensor heating to enhance reliability of radiosonde humidity measurement, in Proceedings of 11th AMS Conference, Dallas, 103–106 (1995)
- A. Paukkunen, New calibration procedure optimizes RS90 radiosonde performance, *Vaisala News* 147. (1998)
- A. Paukkunen, V. Antikainen, H. Jauhiainen, Accuracy and performance of the new Vaisala RS90 radiosonde in operational use, in Proceedings of 11th AMS Symposium on Meteorological Observations and Instrumentation, Albuquerque, New Mexico, 14–18 January 2001
- A. Paukkunen, e.a., Measurement accuracy and repeatability of Vaisala RS90 radiosonde, *Vaisala News* 159, pp 11–13. (2002)
- H.E. Revercomb, e. a., The ARM program's water vapor intensive observation periods. Overview, initial accomplishments, and future challenges, *Bull. Am. Met. Soc.* **84**, 217–236 (2003)
- Z.M. Rittersma, Recent achievements in miniaturised humidity sensors-a review of transduction techniques. *Sensors and Actuators A* **96**, 196–210 (2002)
- P.M. Rowe, L.M. Miloshevich, D.D. Turner, V.P. Walden, Dry bias in Vaisala RS90 radiosonde humidity profiles over Antarctica. *J. Atmos. Ocean. Tech.* **25**, 1529–1541 (2008)
- E. Salasmaa, P. Kostamo, New thin film humidity sensor, in Proceedings of Third Symposium on Meteorological Observations and Instrumentation, Amer. Meteorol. Soc., Washington DC 33–38 1975
- C. Schiller, M. Krämer, A. Afchine, N. Spelten, N. Sitnikov, Ice water content of arctic, midlatitude, and tropical cirrus. *J. Geophys. Res.* **113**, D24208, (2008). doi:10.1029/2008JD010342
- F.J. Schmidlin, A. Ivanov, editors, Radiosonde relative humidity sensor performance: The WMO intercomparison Sept. 1995. Preprint volume. 10th Symposium on Meteorological Observations and Instrumentation. *Amer. Meteorol. Soc.* **68** 71.25 (1998)
- D. Seidel, F. Berger, H. Diamond, J. Dykema, D. Goodrich, F. Immler, W. Murray, T. Peterson, D. Sisterson, M. Sommer, P. Thorne, H. Vömel, J. Wang, Reference upper-air observations for climate: Rationale, progress, and plans, *Bull. Amer. Meteorol. Soc.* **90**, 361–369 (2009). doi:10.1175/2008BAMS2540.1
- H. Smit, W. Sträter, M. Helten, D. Kley, Environmental simulation facility to calibrate airborne ozone and humidity sensors. *Tech. Rep. Juel. Berichte Nr. 3796*, Forschungszentrum Jülich (2000)
- H. Smit, A. Volz-Thomas, M. Helten, H. Pätz, D. Kley, An in-ight calibration method for near real-time humidity measurements with the airborne MOZAIC sensor. *J. Atmos. Ocean. Tech.* **25**, 656–666, (2008). doi:10.1175/2007JTECHA975.1

- R. Smout, J. Elms, D. Lyth, J. Nash, New technology in upper-air observations., in Proceedings TECO-2000 Conference, WMO/TD-1028, Beijing, China, World Meteorological Organization 179–182 (2000)
- D. Sonntag, Advancements in the field of hygrometry, *Meteorol. Zeitschrift*, N. F., 51–66 (1994)
- T. Stickney, M. Shedlov, D. Thompson, Rosemount total temperature sensors, Tech. Rep. 5755, Revision C, Aerosp. Div. Rosemount Inc., Eagan, Minn. (1994)
- T. Suortti, A. Kats, R. Kivi, N. Kämpfer, U. Leiterer, L. Miloshevich, R. Neuber, A. Paukkunen, P. Ruppert, H. Vömel, V. Yushkov, Tropospheric Comparisons of Vaisala Radiosondes and Balloon-Borne Frost-Point and Lyman- $\alpha$  Hygrometers during the LAUTLOS-WAVVAP Experiment. *J. Atmos. Ocean. Tech.* **25**, 149–166, (2008) doi:10.1175/2007JTECHA887.1
- D.D. Turner, B.M. Lesht, S.A. Clough, J.C. Liljegren, H.E. Revercomb, D.C. Tobin, Dry bias and variability in Vaisala RS80-H radiosondes: The ARM experience. *J Atmos. Ocean. Tech* **20**, 117–132 (2003)
- Vaisala, Improved coating of vaisala radiosonde RS92 humidity sensor contact (2007)
- Vaisala, Data continuity (2009), URL <http://www.vaisala.com/weather/products/datacontinuity.html>
- Vaisala, Reference radiosonde program (2010) URL <http://www.vaisala.com/weather/applications/referenceradiosondeprogram.html>
- J. Van Baelen, J.-P. Aubagnac, A. Dabas, Comparison of near-real time estimates of integrated water vapor derived with GPS, radiosondes, and microwave radiometer. *J. Atmos. Ocean. Tech.* **22**, 201–210 (2005)
- S.A. Vay, B.E. Anderson, E.J. Jensen, G.W. Sachse, J. Ovarlez, G.L. Gregory, S.R. Nolf, JR. Podolske, T.A. Slate, C.E. Sorenson, Tropospheric water vapor measurements over North Atlantic during Subsonic Assessment Ozone and Nitrogen Oxide Experiment (SONEX) J. *Geophys. Res.* **105**, 3745–3756 (2000)
- G. Verver, M. Fujiwara, P. Dolmans, C. Becker, P. Fortuin, L. Miloshevich Performance of the Vaisala RS80A/H and RS90 Humicap Sensors and the Meteolabor “Snow White” Chilled-Mirror Hygrometer in Paramaribo, Suriname. *J. Atmos. Ocean. Tech.* **23**, 1506–1518 (2006)
- H. Vömel, H. Selkirk, L. Miloshevich, J. Valverde-Canossa, J. Valdes, E. Kyrö, R. Kivi, W. Stolz, Peng, G. Diaz, J.A., Radiation dry bias of the Vaisala RS92 humidity sensor. *J. Atmos. Ocean. Tech.* **24**, 953–963, (2007a) doi:10.1175/JTECH2019.1
- H. Vömel, V. Yushkov, S. Khaykin, L. Korshunov, E. Kyrö, R. Kivi, Intercomparisons of stratospheric water vapor sensors: FLASH-B and NOAA/CMDL Frost-Point Hygrometer. *J. Atmos. Ocean. Tech.* **24**, 941–952 (2007b) doi:10.1175/JTECH2007.1
- J. Wang, L. Zhang, systematic errors in global radiosonde precipitable water data from comparisons with ground-based GPS measurements. *J. Clim.* **21**, 2218–2238 (2008). doi:10.1175/2007JCLI1944.1
- J. Wang, H.L. Cole, D.J. Carlson, E.R. Miller, K. Beierle, A. Paukkunen, T.K. Laine, Corrections of Humidity Measurement Errors from the Vaisala RS80 Radiosonde - Application to TOGA COARE Data *J. Atmos. Ocean. Tech.* **19**, 981–1002 (2002)
- A. Wexler, Vapor pressure formulation for water in range 0 to 100°C: A revision. *J. Res. Natl. Bur. Stand. U. S., Sect. A.* **80**, 775–785 (1976)
- WMO, *Measurement of atmospheric humidity, in guide to meteorological instruments and methods of observation*, 5th edn. (Tech. Rep. 8, World Meteorological Organization. 1983)
- WMO, *Measurements of upper air temperature, pressure, and humidity. Guide to Meteorological Instruments and Methods of Observation chap. 12*, 7th edn. (WMO No.8, Geneva, 2008)
- K. Yoneyama, M. Fujita, N. Sato, M. Fujiwara, Y. Inai, F. Hasebe, Correction for radiation dry bias found in RS92 radiosonde data during the MISMO field experiment, *SOLA*, **4**, 13–16 (2008)
- M. Zöger, A. Afchine, N. Eicke, M.-T., Gerhards, E. Klein, D. S. McKenna, U. Moerschel, U. Schmidt, V. Tan, F. Tuitjer, T. Woyke, C. Schiller, Fast in-situ stratospheric hygrometers: A new family of balloon-borne and airborne Lyman photofragment uorescence hygrometers. *J. Geophys. Res.* **104**, 1807–1816 (1999)



<http://www.springer.com/978-1-4614-3908-0>

Monitoring Atmospheric Water Vapour  
Ground-Based Remote Sensing and In-situ Methods  
Kämpfer, N. (Ed.)  
2013, VIII, 328 p., Hardcover  
ISBN: 978-1-4614-3908-0